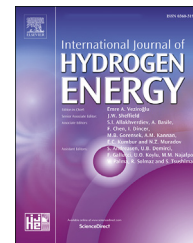




ELSEVIER

Available online at www.sciencedirect.com

ScienceDirect

journal homepage: www.elsevier.com/locate/he

Efficient hydrogen storage with the combination of metal Mg and porous nanostructured material

Hui Liang ^{a,b}, Dandan Chen ^a, Damien Thiry ^b, Wenjiang Li ^{a,**},
Minfang Chen ^{a,*}, Rony Snyders ^{b,c}

^a Key Laboratory of Display Materials and Photoelectric Device (Ministry of Education), School of Materials Science and Engineering, Tianjin University of Technology, 300384 Tianjin, China

^b Chimie des Interactions Plasma-Surface, University of Mons (Umons), 20 Place Du Parc, B 7000, Mons, Belgium

^c Materia Nova Research Centre, 1 Avenue Nicolas Copernic, B 7000 Mons, Belgium

ARTICLE INFO

Article history:

Received 14 March 2019

Received in revised form

21 April 2019

Accepted 22 April 2019

Available online xxx

Keywords:

Porous MWCNTs-PMMA template

Mg nanoparticles

Air-stable

Non-isothermal and isothermal H₂ sorption

Rapid kinetic

High capacity

ABSTRACT

High-energy density and low cost magnesium nanoparticles (Mg NPs)-based material are being sought to meet increasing capable of hydrogen (H₂) storage demand. Here, a kind of air-stable Mg NPs supported on porous structured multi-walled carbon tubes-polymethyl methacrylate (MWCNTs-PMMA) template is prepared owing to reversible well-distributed, dispersed and small-sized Mg/MgH₂ NPs. The aim is to improve the H₂ storage capacity, hydrogen sorption kinetics and thermodynamics of nano Mg-based system without using catalyst. The organic Mg precursor was directly in-situ reduced to metallic Mg NPs in MWCNTs-PMMA template by lithium naphthalide. The size distribution of reduced Mg nanoparticles is around 3.6 ± 0.2 nm, confirmed by XRD and TEM analyses, which is due to the strong interaction between Mg NPs and MWCNTs-PMMA via PMMA binding Mg²⁺, as well as the confinement of porous template hindered the growth and agglomeration of Mg NPs. Moreover, except H₂, O₂ and H₂O molecules can't infiltrate the porous structure of MWCNTs-PMMA resulted in the presence of air stable Mg NPs in the MWCNTs-PMMA. The work provides a new scope to prepare nano metal-based composite for H₂ storage.

© 2019 Hydrogen Energy Publications LLC. Published by Elsevier Ltd. All rights reserved.

Introduction

In recent decades, large-scale application of hydrogen (H₂) energy in efficient storage which has been the most challenging in developing clean energy. Due to their high hydrogen storage capacity, Magnesium (Mg)-based materials as the safe and efficient solid-state hydrogen storage are an attractive option. Therefore, to prepare Mg based hydrogen storage materials in a highly efficiency and controllable

method is becoming a meaningful works for sustainable development. Many methods have been developed to try to ensure hydrogen uptake and release close to theoretical capacity of 7.6 mass% and 110 g L⁻¹ below 100 °C without using the heavy metal catalyst [1–6]. Recently, due to the abundance, low cost, low density, low toxicity, high hydrogen capacity and high efficiency sorption property, considerable efforts have been made on the design and formation of size confined magnesium nanoparticles (Mg NPs)-based material as one efficient candidate for hydrogen storage by decreasing

* Corresponding author.

** Corresponding author.

E-mail address: mfchentj@126.com (M. Chen).

<https://doi.org/10.1016/j.ijhydene.2019.04.212>

0360-3199/© 2019 Hydrogen Energy Publications LLC. Published by Elsevier Ltd. All rights reserved.

diffusion path lengths for hydrogen and decreasing the required thickness of MgH₂ layer [7–9]. For example, Sun et al. concluded the current state of Mg based materials for hydrogen storage, demonstrating nanosized magnesium has the potential to achieve the favourable thermodynamics and rapid kinetic for uptake/release H₂ [10]. Kim et al. presented the dimensional effect of nanostructured Mg/MgH₂ on hydrogen storage applications, showing that the correlation of size and sorption temperature/pressure, in which the smaller nanosized metal might have more rapid kinetic and better thermodynamics than bulk Mg [3]. Paskevicius et al. proved that the size of MgH₂ supported on porous carbon made a much pronounced effect on the H desorption temperature, which could be decreased from below 240 °C–200 °C with the reducing the particle size from ~7 nm to 0.9 nm. Therefore, the fabrication of H₂ storage material should be focused on smaller-size, stable structure, higher reversible storage capacity, as well as mild operation conditions of temperature and pressure [5,7–9]. As is well known, the carbon materials as supported and additive material can confine and hinder the growth and agglomeration of metal NPs, which have attracted more and more interest in exploiting H₂ storage or energy material [11–21,47–50]. For example, Yuan et al. used multi-wall carbon nanotubes (MWCNTs) to support nano Pd particles obtained by solution chemical reduction for efficient hydrogen storage of magnesium hydrides, showing porous carbon as a supporter could disperse Pd particle and improve the storage kinetic of nanocomposite [48]. Yuen et al. demonstrated that porous carbon aerogels could prevent further growth of MgH₂ nanoparticles, and decrease its hydrogen desorption temperature [20]. Hou et al. studied that the hydrogen storage property of metal Mg impregnated on the porous channels of activated charcoal scaffold and found that the physical contributions of CNTs for hydrogen storage is to provide the fast diffusion surface/channels to reach Mg-based hydrides [21]. Tian et al. investigated the H₂ storage kinetics of Mg-based composites, which were significantly improved by combining various types of carbon with metal Mg, and achieved the lowest dehydrogenation temperature of 180 °C [22].

Although nanoconfinement in porous carbon scaffold has been widely considered as a potential method to improve the sorption performance of nano Mg particle, the existed major issues of nanosized Mg supported in carbon scaffold materials still are the uncontrollable pore filling and low degree of Mg/MgH₂ loading [23–26]. Jongh et al. found that it was hard for metal Mg to directly enter the pores of the porous carbon as a scaffold system by melt infiltration method, resulted the Mg amount loaded was confined [27]. Meanwhile, some carbon materials like CNTs were considered to be insoluble for most organic solvents because of the easy aggregation, which limited the applications of the novel wet-phase method [28–30]. And some functional groups such as –COOH, –OH, and –CJO have been modified on the surface of CNTs to avoid the aggregation, which could also be acted as nucleation sites of metal ions. However, the chemical modification approach often led to the extreme degradation of the tube structure of CNTs [31–33]. In order to disperse CNTs in solutions and prepare CNTs-metal NPs composite, some polymers can be as the bridge for the binding of metal nanoparticles and CNTs.

Jaime et al. used polyvinyl pyrrolidone (PVP) as the surfactant to modify metal Pd and bimetallic Ni₅₀Pd₅₀ nanoparticles, and deposited the above NPs on CNTs via the reduction-by-solvent method [34,35]. Using the similar methods, the other CNTs-metal NPs composite such as SWNTs-PSMA-Pd NPs, SWNT-Pt-PANI and CNT-CdS-oleylamine also have been prepared [36–38]. On the other hand, air-stable structure of Mg composite is important rule for hydrogen storage. Jeon et al. prepared an air-stable nano metal Mg/PMMA composite as the high-capacity H₂ storage materials using bis (cyclopentadienyl) magnesium (Cp₂Mg) as Mg precursor, which was dangerous and explosive in air [24,39]. Tirandai et al. used methyl magnesium chloride (MeMgCl) as a safe and efficient Mg precursor to prepare SWCNTs-Mg NPs composite by solution reduction method, the obtained Mg NPs in the diameter of 3–5 nm presented the potential in H₂ storage [40]. In a previous study, we also successfully used MeMgCl as precursor to produce an air-stable Mg NPs/PMMA composite to be an efficient H₂ storage materials. In the work, the prepared MWCNTs-PMMA complex as the template to support MeMgCl as Mg precursor, then, the organic Mg precursor was directly in-situ reduced to well-dispersed metallic Mg NPs in MWCNTs-PMMA template by lithium naphthalide. MWCNTs-PMMA template played an efficient role for preventing the oxidation of Mg NPs because O₂ and H₂O molecules couldn't infiltrate the porous structure of MWCNTs-PMMA. X-ray spectroscopy (XRD) and transmission electron microscope (TEM) give a powerful evidence for Mg NPs were protected from O₂ and H₂O in MWCNTs-PMMA template, showing the porous structure of PMMA gel can infiltrate H₂ molecules rather than O₂ and H₂O molecules [5,24,39,41]. The Fourier transform infrared (FT-IR) and Raman spectra proved carboxylate functional group of PMMA might act as a capping ligand to prevent the aggregate of Mg NPs and the curling of tubes. The mobility of Mg²⁺ were controlled by the strong chemical interaction bond between the Mg²⁺ and MWCNTs-PMMA. The formation mechanism between Mg NPs and MWCNTs-PMMA was proposed. We found that the thriving porous structured MWCNTs-PMMA gave a significant influence on the amount and dispersion of Mg NPs. The obtained Mg NPs in the diameter of 3–4 nm loaded in the highly channel-nanosized network of MWCNTs-PMMA, showed a high H₂ storage capacity, rapid kinetics, unstable thermodynamic and reversibility absorption/desorption cycle. The solution-phase synthesis of MWCNTs-PMMA-Mg composite can be generally applied to a novel H₂ storage materials.

Experimental

Materials

Multi-walled carbon nanotubes (MWCNTs) with an inter diameter of 3–5 nm and a length of 30 μm, PMMA (resistant to high temperature, Mw = 120,000), Methyl magnesium chloride (3.0 M solution in THF), lithium, and naphthalene were purchased from Sigma-Aldrich. Anhydrous tetrahydrofuran (THF, 99.8%) used as solvent in the polymerization reaction was obtained from Aladdin chem. Ltd.

Synthesis of MWCNTs-PMMA-Mg NPs composites

All samples were prepared in an inert atmosphere (Ar-filled glove box). The synthesis process is as follows: Firstly, the mixture of MWCNTs, PMMA, MeMgCl and THF solution were added into 100 mL 3-neck round bottom flask, after refluxing and mechanical stirring for 1 h, the MWCNTs-PMMA complexes were formed in presence of Mg^{2+} precursor from MeMgCl, which was named Solution A. Meanwhile, naphthalene (1 eq.), Li (1 eq.), and THF were added into another 100 mL of 3-neck round bottom flask, after refluxing and mechanical stirring at 60 °C for 2 h, Li-naphthalene compound was obtained, which was named Solution B. Secondly, the solution B was added into the solution A, after refluxing and stirring at 55 °C for 24 h, the Mg ions might be reduced to metal Mg nucleus and further aggregated nanoparticles along MWCNTs by Li-naphthalene. Finally, after cooling to room temperature, washing with THF solution for three times, isolating by centrifugation, and drying under an Ar atmosphere, the final product of MWCNTs-PMMA-Mg NPs composite (MPMC) was obtained and stored in vacuum drying oven for future characterization and analysis. In order to investigate the loading Mg amount, the effect of the MWCNTs and PMMA used in the experiment were studied and summarized in Table 1 the optimal ratio of MWCNTs:MeMgCl:PMMA is 0.15 g:5 ml:0.2 g, in which more Mg NPs with less MWCNTs and PMMA could be loaded on MWCNTs-PMMA template related to the yield of Mg NPs. The following sample of MPMC-4 as a representative was further studied in detail.

Characterization

The morphology and composition of the samples were analyzed by transmission electron microscope (TEM, FEI TALOS F200 X). The microstructures of the samples were characterized in an air-sensitive sample holder by X-ray powder diffraction (XRD, Rigaku D/max/2500 PC, Japan) using $CuK\alpha$ radiation with $\lambda = 1.5418 \text{ \AA}$ operating at 40 kV/100 mA with a scanning speed of 8°/min in the 2 θ range from 10 to 70°. Raman analysis was carried out using Horiba Evolution-High resolution laser confocal microscopic Raman spectrometer (produced by Horiba Jobin Yvon SAS) with a spectrometer focal length of 800 mm and aberration correction using Czerny-Turner. Fourier transform infrared (FT-IR) spectra were obtained from KBr pellets using Frontier Mid-IR FTIR/STA6000-TL9000-MS (produce by Perkin Elmer) in the range of 4000–400 cm^{-1} , with a spectral resolution of 4 cm^{-1} and an average of 32 scans. FTIR analysis was performed to obtain qualitative estimations of the changes of functional groups of Mg-based composite compare to MWCNT-PMMA.

H₂ absorption-desorption experiments

After drying in vacuum environment for >24 h to remove solvent. The uptake/release H₂ for the reduced Mg NPs dispersed in gas selective system of MWCNTs-PMMA (MPMC-4 sample) were measured using, the non-isothermal/isothermal H₂ sorption method, and the schematic of hydrogen storage system was shown in Scheme 1.

Temperature programmed reduction and desorption tests

Non-isothermal hydrogen sorption of the samples were studied with temperature programmed absorption/desorption (H₂-TPR-TPD) cycle by Autosorb-IQ3+ ChemStar (produce by Quantachrome) with a TCD detector, which was attached with a quartz reactor in a tube furnace. Approximately 100 mg of the sample was used for each measurement. Argon was used as the carrier gas and all composite samples were heated up to 400 °C (pure Mg was heated up to 600 °C) with 5 °C/min in 25 mL/min Ar-flow.

H₂ absorption-desorption experiments with high pressure

Isothermal hydrogen sorption were performed in a high pressure gravimetric analyzer at certain temperature in the range of from 0.01 bar to 80 bar by HPVA-II high pressure absorption equipment (Micromeritics company, USA). Before performing the isotherms, in the gravimetric apparatus, the samples were pretreatment under vacuum at 200 °C, respectively.

All sorption kinetic measurements of MPMC were evaluated using an PCT hydrogen generating equipment (produce by Tong Yuan Heng Li) combine with hydrogen generator (PGH-300, produce by Pu Lai xi technology company, Bei Jin) and gas chromatograph (GC126, produce by instrument analysis company, Shang Hai). For the absorption/desorption cycling, before starting the next absorption cycle, the sample was kept at 200 °C in vacuum for several hours to allow full hydrogen desorption.

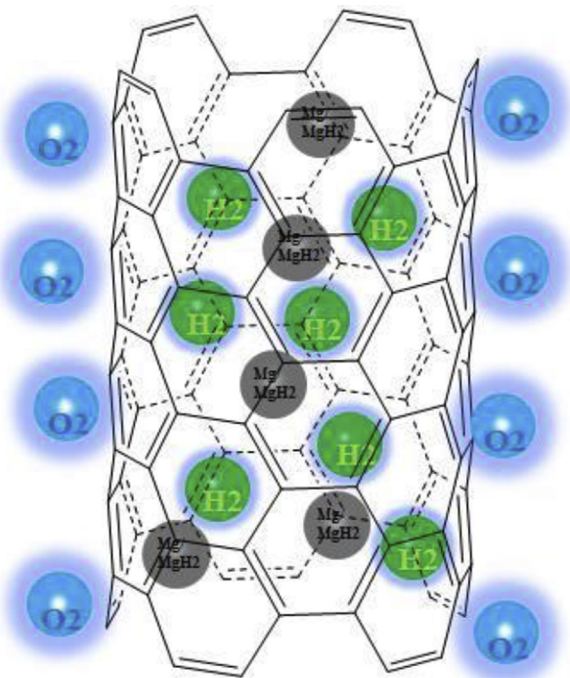
Results and discussion

High transmission electron microscope

Fig. 1 shows the TEM images of MWCNTs-Mg NPs (a,e) and MPMC (b,c,d,f), respectively. Mg NPs were distributed uniformly on the surface of MWCNTs-PMMA, of an approximately spherical morphology with diameter of about 3.8 nm as shown in diameter fraction (Fig. 1h). Refer to TEM images of

Table 1 – Detailed information of the samples.

Sample	Weight of MWCNTs(g)	MeMgCl (ml)	Weight of PMMA(g)	The yeild of Mg NPs(wt%)
MWCNTs-Mg NPs-1	0.02	5	0	51.6%
MPMC -2	0.05	5	0.10	75%
MPMC-3	0.10	5	0.15	80%
MPMC-4	0.15	5	0.20	81.3%
MPMC-5	0.20	5	0.30	82.0%
MPMC-6	0.25	5	0.40	82.0%



Scheme 1 – Schematic of hydrogen storage MPMC material: high-capacity Mg NPs are in situ synthesized and supported by a selectively gas-permeable matrix.

MPMC (Fig. 1b), we also can observe MWCNTs were dispersed uniformly in PMMA phase and the more Mg NPs were dispersed and grown along the MWCNT compare with the image of MWCNTs-Mg NPs composite (Fig. 1a). Moreover, from Fig. 1c and d, the well-distributed Mg NPs are loaded on the MWCNTs-PMMA template, and there is about 20 nm space between the particles, which might contribute to decrease the chain reaction effect of MgH and to improve the H₂ sorption kinetic of composite. Fig. 1e shows the presence of lattice fringes with a separation of 0.30 nm in agreement with the (101), inter planar d spacing of hexagonal magnesium in MWCNTs-Mg NPs composite, while the Mg NPs in MPMC had two kinds of lattice fringes with a separation of 0.30 nm and 0.287 nm in agreement with the (101) and (002) because encapsulation of PMMA lead to the appearance of (002) (Fig. 1f). The EDS data (Fig. 1g) indicated that no byproduct such as chlorinated impurities are presented, so the fabrication technique was favorable to produce high purity Mg NPs.

X-ray diffraction

As shown in Fig. 2, the XRD pattern of MPMC (exposure to air for 10 days) exhibits a two-phase (crystalline and amorphous) structure: peaks located at $2\theta = 25.6^\circ, 32.2^\circ, 34.4^\circ, 36.6^\circ, 43.15^\circ, 47.8^\circ, 57.4^\circ$ and 63.1° were assigned to (100), (002), (101), (102), (110) and (103) planes of hexagonal magnesium, peaks located at $2\theta = 25.6^\circ$ and 43.15° were assigned to the amorphous peaks of MWCNTs, and the peak at $2\theta = 21.9^\circ$ was assigned to the amorphous peak of PMMA according with Supplementary Fig. 1, there were no peaks of MgO and Mg(OH)₂ after 10 days

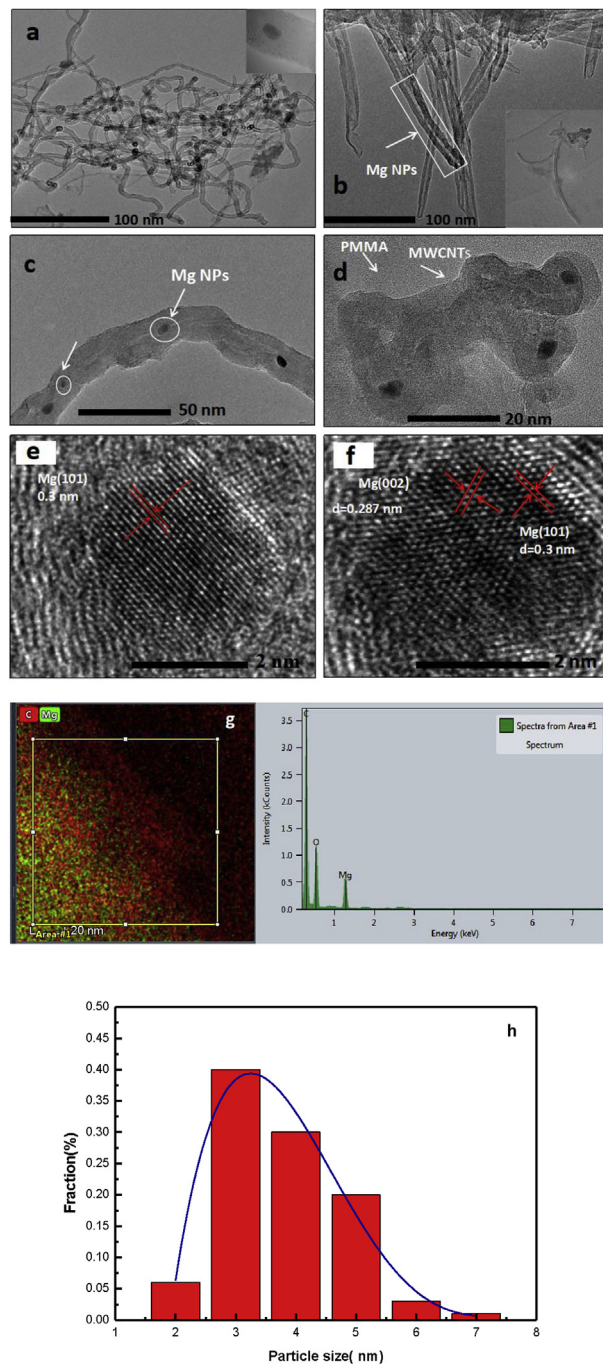


Fig. 1 – HR-TEM micrograph of MWCNTs-Mg NPs composite (a),(e) and MPMC (b),(c),(d),(f), respectively; EDS spectrum and fraction-size of MWCNTs-PMMA indicated the presence of magnesium (g,h).

of air exposure, suggesting PMMA can protect Mg NPs from O₂ and H₂O. As using the well-know scherrer's formula calculation, grain-particle size of Mg nanoparticles encapsulated in PMMA was about 3.6 ± 0.2 nm, and this agreed well with the analysis made from TEM micrography. Refer to the XRD pattern of the MWCNTs-PMMA-Mg/MgH₂ NPs composite after performed H₂ absorption/desorption cycle, presenting the same stable crystal morphology with as-synthesized MPMC, there were peaks of MgH₂ at $2\theta = 29.6^\circ, 32.5^\circ, 34.9^\circ, 42.8^\circ,$

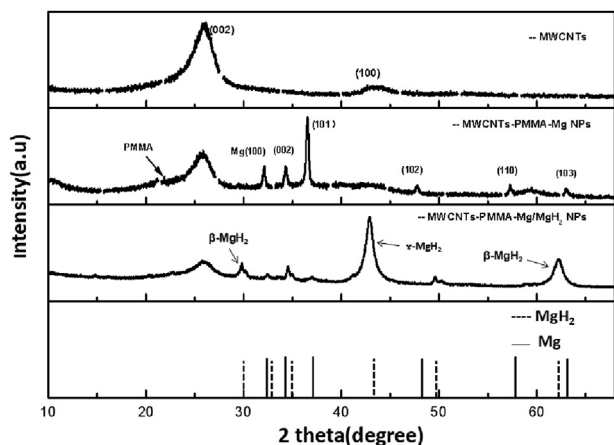


Fig. 2 – X-ray diffraction patterns of MWCNTs and MPMC and MWCNTs-PMMA-Mg/MgH₂ NPs for absorption/desorption cycle.

49.5° and 62.16°, including the β and γ peaks of MgH₂ were observed previously in the XRD patterns. According with the reported article, it was attributed to the Mg NPs supported on MWCNTs adsorbed H₂ at high pressure lead to the appearance of the β and γ peaks [42], as well as several weakened Mg NPs peaks and MWCNTs peaks also were observed because of its low abundance (Fig. 2).

Raman spectra

The Raman spectroscopy is an alternative method for analyzing the damage degree of MWCNTs supported Mg NPs (Fig. 3). There are two particularly important peaks in the range of 1340–1570 cm⁻¹ of the spectrum, the sharp band located at around 1570 cm⁻¹ (G band) is attribute to the in-plane vibration of the C–C bond [42], while the band at 1340 cm⁻¹ (D band) is used to analysis the presence of disorder in carbon system [42]. The relative intensity ratio of the D to the G bands can provide information of MWCNTs structural defects, with the ratio of I_D/I_G increasing, the defect of

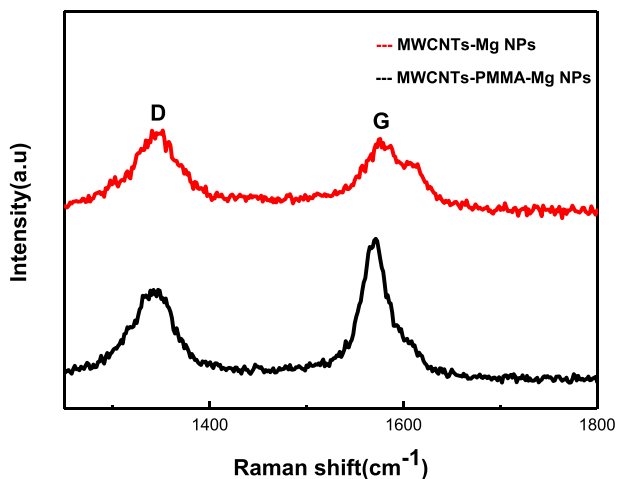


Fig. 3 – Raman spectra of MWCNTs-Mg NPs and MPMC.

MWCNTs were increased in the composites [15,34,41]. The I_D/I_G ratio of MPMC and MWCNT-Mg NPs composite was 0.8 and 1.05, respectively. The intensity of D band decreased in MWCNTs-Mg NPs composites is attributed to the presence of Mg NPs, causing a debundling effect of the nanotubes according with the reported article [40,43]. While Mg NPs were deposited on MWCNTs-PMMA template, the debundling of the nanotubes was avoided, MWCNTs present a few defect, contributed to more Mg NPs were loaded on MWCNTs-PMMA template, these results also could be observed in HETEM images, it was clearly shown that PMMA could protect tube-wall from destroying to load more Mg NPs.

Fourier-transform infrared spectroscopy

FTIR analysis of the synthesized nanocomposites was performed to obtain qualitative estimations of the changes of functional groups of MPMC compare to MWCNTs-PMMA. FTIR spectra of MWCNTs, MWCNTs-Mg NPs and MPMC are shown in the Fig. 4, the absorption band of PMMA at 1734 cm⁻¹ is assigned to C=O stretch, but absent in MPMC due to the conjugation effect by attachment of Mg NPs to the ring structure of MWCNTs wall or at tube ends [44]. This is an evidence of the successful formation of interactions bond and charge-transfer between Mg NPs and MWCNTs-PMMA. The absorption peak of PMMA at 1239 cm⁻¹ is assigned to –CH₂-twisting, but the peak location in MPMC moved to 1233 cm⁻¹ and the intensity of peak also has weakened, which may be explained to Mg ions were attracted to MWCNTs-PMMA through electrostatic attraction to the formation of π-π bonding between Mg NPs and MWCNTs-PMMA in THF solution. The bands correspond to C–O of the methoxy group in pure PMMA appeared at 1151 cm⁻¹, the absorption peak in MPMC has weakened due to Mg²⁺ was attracted to the acrylate of PMMA [39]. There are also evidences of the peak at 989 cm⁻¹ was assigned to –C–O–C– in PMMA, but absent in MPMC due to the O]C–OCH₃ bond of MMA was dissociated and coordinate to stable oxygen radical attract with Mg NPs [45]. The absorption peak at 1045 cm⁻¹ in MWCNTs is assigned to O–C]O symmetric and asymmetric stretching vibrations, while the

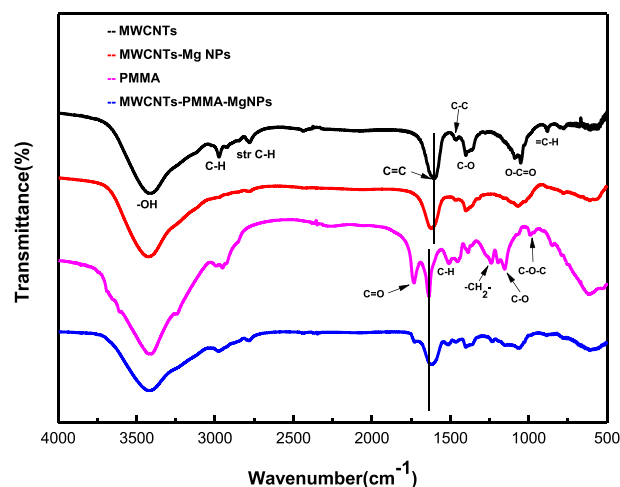


Fig. 4 – FTIR spectra for MWCNTs, MWCNTs-Mg NPs, PMMA and MPMC, respectively.

peak in MWCNTs-Mg NPs and MPMC moved to 1058 cm^{-1} and the intensity of peak also has weakened due to deformation of the carboxylic acid group [44,46], resulting from the presence of Mg NPs causing a debundling of the nanotubes also was observed in Raman spectrum.

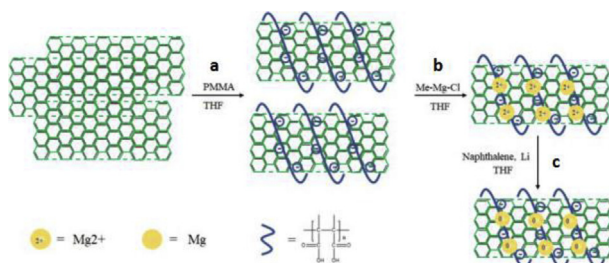
Synthesized mechanism of MPMC

Refer to these characterization results, the one-pot reduction reaction of methyl magnesium chloride as Mg precursor, PMMA as surfactant to disperse MWCNTs was an effective, inexpensive and achievable method for the fabrication of MPMC, PMMA provided a gas-selective polymer barrier to make the Mg NPs uptake and release hydrogen without oxidizing. The synthesized mechanism of MPMC for the process was explained and shown in Scheme 2, the MWCNTs were dispersed with soluble PMMA, and Mg^{2+} initially attracted to MWCNTs-PMMA complexes through electrostatic interactions, may coordination interaction with acrylate ions of MMA and slowly shift the binding mode to charge-transfer interaction with MWCNTs in THF solution (Scheme 1a and b), and subsequently MWCNTs-PMMA complexes matrix prevented the reduced Mg NPs from aggregating with each other (Scheme 1c). The reduced Mg nanoparticles modified with MMA monolayer and they were dispersed uniformly on the MWCNTs-PMMA template. Moreover, PMMA has additional effect on confining MgH_2 -MWCNTs interface to enhance the H_2 desorption kinetic of composite.

Hydrogen storage

Non-isothermal H_2 sorption

All samples were dried and reduced pretreatment at $200\text{ }^\circ\text{C}$ before non-isothermal hydrogen sorption measurement. Hydrogen temperature programmed absorption/desorption experiments were performed for MPMC and pure Mg (Fig. 5). The H_2 -TPR profiles were obtained by reducing samples in the range from room temperature to $600\text{ }^\circ\text{C}$ at 101 kPa as shown in Fig. 5a, MPMC exhibits the highest absorption peak temperature of $238\text{ }^\circ\text{C}$, which is prominent lower than pure Mg, presenting the highest absorption peak temperature of $418\text{ }^\circ\text{C}$. The absorption peak of MPMC presents a sharp peak compared to broad peak of pure Mg, implying that hydrogen absorption kinetics of Mg NPs supported on MWCNTs-PMMA was improved obviously and more rapid than the reported article [4–9,13–17,24–26,39]. With respect to the onset



Scheme 2 – Synthesis mechanism of MPMC.

temperature, MPMC has the start absorption temperature of $150\text{ }^\circ\text{C}$, suggesting Mg NPs could achieve lower absorption temperature for the feasible MPMC hydrogen storage system.

For the H_2 -TPR-TPD cycle experimental, after non-isothermal hydrogen absorption measurement, then scavenging H_2 for 60 min, non-isothermal hydrogen desorption of pure Mg crystal and MPMC were investigated by temperature programmed control desorption with TPD-TCD (Fig. 5b) in the temperature range room temperature to $600\text{ }^\circ\text{C}$ with 0 bar H_2 using argon as the carrier gas, MPMC enabled start to release hydrogen as low as $120\text{ }^\circ\text{C}$ with the highest desorption peak temperature of $240\text{ }^\circ\text{C}$, much lower than pure Mg crystal, presenting the highest desorption peak temperature of $416\text{ }^\circ\text{C}$, implying Mg NPs encapsulated in porous structured MWCNTs-PMMA template could release H_2 in lower temperature, conforming to industrial application [25]. Refer to H_2 desorption peak, there is a clear difference in the shape of pure Mg and MPMC, in which MPMC presents a more sharp peak compared to pure Mg, suggesting MPMC has more rapid H_2 desorption kinetics, which will be analyzed detail in the following absorption/desorption cycle test. As integral calculation for desorption peak area, MPMC release 4.5 wt\% of H_2 at $240\text{ }^\circ\text{C}$, and release about 3.7 wt\% of H_2 absolutely at $150\text{ }^\circ\text{C}$. Then depend on the calculation results, we also investigated the H_2 desorption amount of composite at $150\text{ }^\circ\text{C}$ by ab/desorption cycling measurement.

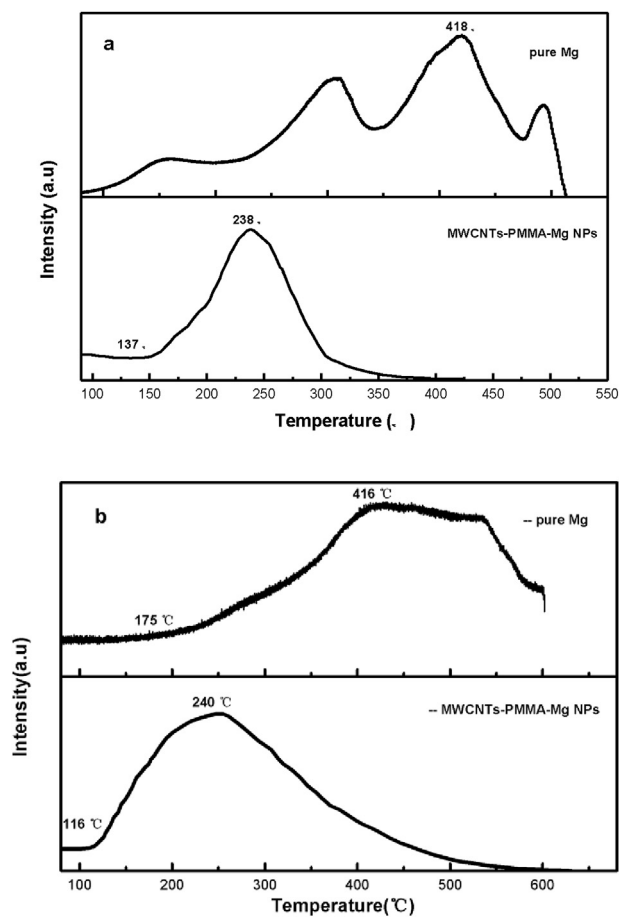


Fig. 5 – Hydrogen absorption and desorption during TPR (a) and TPD (b) cycles observed on MPMC and pure Mg.

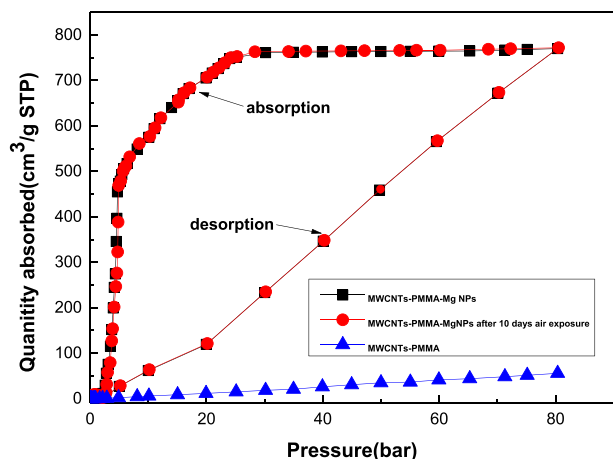


Fig. 6 – Isothermal H₂ Quantity Adsorbed of MPMC (0 day and 10 days exposure to air) and MWCNTs-PMMA assembles with various pressure using HPVA-II.

Isothermal hydrogen sorption

Isothermal hydrogen sorption were investigated by the pressure programmed control absorption/desorption measurement with HPVA-II equipment using argon as the carrier gas. In this paper, as consider the research status, we focused on H₂ absorption/desorption of material within 200 °C for exploring application widely in industry. In Fig. 6, H₂ absorption amount of MPMC with various pressure ranging from 0.01 bar to 80 bar at 200 °C were demonstrated, exhibiting the hydrogen absorption amount of 7.1 wt% (750 cm³/g STP) for Mg NPs at 200 °C with the pressure reaching to 80 bar, with a sharp weight increase within 10 bar and continue increasing obviously within 25 bar, then increase slowly in rang from 25 to 80 bar. Meanwhile, the isothermal high pressure H₂ sorption of MPMC air-exposed for 10 days shows a similar pattern with the as-synthesized MPMC, demonstrating the air-exposure composite could keep the stable hydrogen sorption performance. On the other hand, the hydrogen absorption amount of MWCNTs-PMMA assembles only is 0.2–0.5 wt% (about 40 cm³/g STP) at 200 °C with pressure increasing from 0.01 to 80 bar, indicating that the physiorption of hydrogen molecules in MWCNTs-PMMA via van der Waals bonds is much lower than that of MPMC, consistence with the previous report., [46]. The results proved that Mg/MgH₂ NPs in MWCNTs-PMMA was the main reason for the uptake/release hydrogen.

The sorption kinetic profiles of samples were shown in Fig. 7, depend on the above H₂-TPR-TPD cycle and isothermal high pressure hydrogen sorption, we investigated the hydrogen absorption capacity and hydrogen absorption rate within 200 °C and 20 bar H₂ for MPMC using a PCT equipment. Refer to the absorption isotherm measurement, MPMC accomplished a higher hydrogen absorption amount of 6.7 wt % and higher absorption rate within 8 min at 20 bar and 200 °C, displayed a sharp weight increase upon hydrogen exposure to 20 bar at 200 °C with a steep slope of hydrogenation occurring during the first 5 min and plateaus off to a constant mass in <30 min. The air-exposure MPMC also show the similar performance with the composite exposure to air for 0 day. In

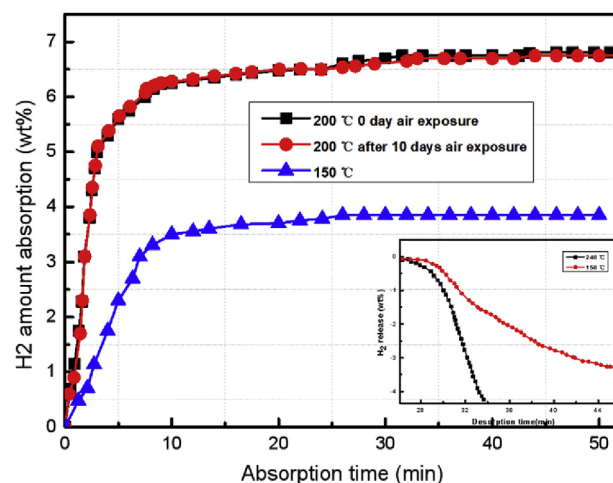


Fig. 7 – Hydrogen absorption of MPMC (0 day and 10 days exposure to air) at 150 °C and 200 °C, respectively, with a pressure of 20 bar; Inset: desorption kinetic curves of MPMC at 150 and 240 °C with 0 bar H₂.

comparison, at 20 bar and 100 °C, MPMC has lower hydrogen absorption amount of 3.5 wt% and slower absorption kinetic, pure Mg only has hydrogen absorption amount of 1.75 wt% at 200 °C and 20 bar H₂ and even no H₂ absorption at 25 °C because its stable absorption thermodynamic (supplementary Fig 2). In Fig. 7, refer to the inset figure, throughout long absorption/desorption cycles, MPMC released about 3.7 wt% of hydrogen at 0 bar H₂ and 150 °C within 20 min and released about 4.2 wt% of hydrogen at 0 bar and 240 °C within 10 min. On the other hand, MPMC has better reversibility and long life and well-preserved H₂ storage capacity. So Mg NPs were loaded on MWCNTs-PMMA assembles could achieve an excellent H₂ storage performance.

Conclusion

A nanosized Mg NPs supported on porous structured MWCNTs-PMMA template, is designed to a satisfy H₂ storage demand based on our previous experiment. It is potential to shift from bulk metal to excellent air-stable H₂ storage performance materials without using catalyst, which can considerably improve the thermodynamic and kinetic properties, as well as overcome high reactivity of metallic Mg to O₂ and H₂O. The synthesis mechanism mode of MPMC was proposed, contributed to in-depth understanding the fundamental mechanism of hydrogen storage. PMMA as dispersing reagent in solution and capping ligands to confine the size of Mg NPs, whereas the porous structure of the MWCNTs-PMMA serves as hydrogen diffusion channels. Mg NPs support on porous MWCNTs-PMMA template, achieving hydrogen absorption capacity of 6.7 wt% at 20 bar and 200 °C, which was very close to theoretical capacity of 7.6 mass%. The composite could release 3.7 wt% of H₂ at 150 °C and 0 bar H₂, show a faster desorption kinetic than reported material. More of that, the composite sample could perform a reversible stabilized uptake/release cycles. More of that, the composite sample could perform a reversible stabilized uptake/release cycles. This work

will encourage further studies on the efficient H₂ storage material in combining metal and porous organic/inorganic material to promote the development of sustainable clean energy.

Acknowledgements

This work was supported by the Joint Foundation of National Natural Science Foundation of China (Grant No. U1764254), China; the National Natural Science Foundation of China (51871166); 321 Talent Project of Nanjing (Grant No. 631783), China; 111 Project (D17003), China.

Appendix A. Supplementary data

Supplementary data to this article can be found online at <https://doi.org/10.1016/j.ijhydene.2019.04.212>.

REFERENCES

- Kim DR, Cho KW, Choi YI, et al. Fabrication of porous Co-Ni-P catalysts by electrodeposition and their catalytic characteristics for the generation of hydrogen from an alkaline NaBH solution. *Int J Hydrogen Energy* 2009;34(6):2622–30.
- Momirlan M, Veziroglu TN. The properties of hydrogen as fuel tomorrow in sustainable energy system for a cleaner planet. *Int J Hydrogen Energy* 2005;30(7):795–802.
- Sadhasivam T, Kim HT, Jung S, Roh SH, Park JH, Jung HY. Mg/MgH₂ for hydrogen storage applications: a review. *Renew Sustain Energy Rev* 2017;72:523–34.
- Khaselev O, Turner JA. A monolithic photoelectrochemical device for hydrogen production via water splitting. *Science* 1998;280(5362):425–7.
- Chaubey R, Sahu S, James OO, Maity S. A review on development of industrial processes and emerging techniques for production of hydrogen from renewable and sustainable sources. *Renew Sustain Energy Rev* 2013;23:443–62.
- Haas I, Gedanken A. Synthesis of metallic magnesium nanoparticles by sonoelectrochemistry. *Chem Commun* 2008;15:1795–7.
- De Jongh PE, Wagemans RW, Eggenhuisen TM, Dauvillier BS, Radstake PB, Meeldijk JD, Geus JW, De Jong KP. Reversible hydrogen storage in Mg(BH₄)₂/carbon nanocomposites. *Chem Mater* 2007;19(24):6052–7.
- Tao SX, Notten PHL, Van Santen RA, Jansen APJ. First-principles predictions of potential hydrogen storage materials: nanosized Ti(core)/Mg(shell) hydrides. *Phys Rev B* 2011;83(19):195403.
- Ellinger FH, Holley CE, McInteer BB, Pavone D, Potter RM, Staritzky E, Zachariasen WH. The preparation and some properties of magnesium hydride. *J Am Chem Soc* 1955;77(9):2647–8.
- Cai WP, Zhou XS, Xia LD, Jiang KL, Peng SM, Long XG, Liang JH. Positive and negative effects of carbon nanotubes on the hydrogen sorption kinetics of magnesium. *J Phys Chem C* 2015;119(45):25282–90.
- Tzitzios V, Georgakilas V, Oikonomou E, Karakassides M, Petridis D. Synthesis and characterization of carbon nanotube/metal nanoparticle composites well dispersed in organic media. *Carbon* 2006;44(5):848–53.
- Basiuk VA, Basiuk EV. Chemistry of carbon nanotubes. 2008.
- Rodrigues EG, Carabineiro SAC, Delgado JJ, Chen X, Pereira MFR, Orfao JJM. Gold supported on carbon nanotubes for the selective oxidation of glycerol. *J Catal* 2012;285(1):83–91.
- Rodrigues EG, Delgado JJ, Chen X, et al. Selective oxidation of glycerol catalyzed by gold supported on multiwalled carbon nanotubes with different surface chemistries. *Ind Eng Chem Res* 2012;51(49):15884–94.
- OConnell MJ, Bachilo SM, Huffman CB, Moore VC, Strano MS, Haroz EH, Rialon KL, Boul PJ, Noon WH, Kittrell C, Ma J, Hauge, Weisman RH, Smalley RE. Band gap fluorescence from individual single-walled carbon nanotubes. *Science* 2002;297(5581):593–6.
- Ozawa H, Yi X, Fujigaya T, Niidome Y, Asano T, Nakashima N. Supramolecular hybrid of gold nanoparticles and semiconducting, single-walled carbon nanotubes wrapped by a PorphyrinFluorene copolymer. *J Am Chem Soc* 2011;133(37):14771–7.
- D'Souza F, Kadish KM, editors. Handbook of carbon nano materials. Hackensack, NJ: World Scientific; 2011.
- Guldi DM, Martin NE. Carbon nanotubes and related structures. 2010.
- Akasaka T, Wudl F, Nagase S. Chemistry of nanocarbons. Chichester: John Wiley & Sons; 2010.
- Yuen SA, Margo KO, Subramanian S, Pieter CMMM, J Krijn PD, Petra EDJ. The size dependence of hydrogen mobility and sorption, kinetics for carbon-supported MgH₂ particles. *Adv Funct Mater* 2014;24(23):3604–11.
- Hou PX, Xu ST, Ying Z, Yang QH, Liu C, M Cheng H. Hydrogen adsorption/desorption behavior of multi-walled carbon nanotubes with different diameters. *Carbon* 2003;41(13):2471–6.
- Tian M, Shang CX. Mg-based composites for enhanced hydrogen storage performance. *Int J Hydrogen Energy* 2019;44:338–44.
- Tzitzios V, Georgakilas V, Oikonomou E, et al. Synthesis and characterization of carbon nanotube/metal nanoparticle composites well dispersed in organic media. *Carbon* 2006;44(5):848–53.
- Jeon KJ, Theodore A, Wu CY, et al. Hydrogen absorption/desorption kinetics of magnesium nano-nickel composites synthesized by dry particle coating technique. *Int J Hydrogen Energy* 2007;32(12):1860–8.
- Jain IP, Lal C, Jain A. Hydrogen storage in Mg: a most promising material. *Int J Hydrogen Energy* 2010;35(10):5133–44.
- Ellinger FH, Holley CE, McInteer BB, Pavone D, Potter RM, Staritzky E, Zachariasen WH. The preparation and some properties of magnesium Hydride1. *J Am Chem Soc* 1955;77(9):2647–8.
- Jongh PED, Wagemans RWP, Eggenhuisen TM, Dauvillier BS, Radstake PB, Meeldijk JD, et al. The preparation of carbon-supported magnesium nanoparticles using melt infiltration. *Chem Mater* 2007;19(24):6052–7.
- Zhao LP, Gao L. Novel in situ synthesis of MWNTs-hydroxyapatite composites. *Carbon* 2004;42(2):423–60.
- Ozawa H, Yi X, Fujigaya T, Niidome Y, Asano T, Nakashima N. Supramolecular hybrid of gold nanoparticles and semiconducting, single-walled carbon nanotubes wrapped by a PorphyrinFluorene copolymer. *J Am Chem Soc* 2011;133(37):14771–7.
- Dominguez SD, Murcia AB, Amoros DC, Solano AL. Semihydrogenation of phenylacetylene catalyzed by metallic nanoparticles containing noble metals. *J Catal* 2006;243(1):74–81.
- Hernadi K, Ljubovic E, Seo JW, Forro L. Synthesis of MWNT-based composite materials with inorganic coating. *Acta Mater* 2003;51(5):1447–52.

- [32] Wang D, Li ZC, Chen LW. Templated synthesis of single-walled carbon nanotube and metal nanoparticle assemblies in solution. *J Am Chem Soc* 2006;128(47):15078–9.
- [33] Balasubramanian K, Burghard M. Chemically functionalized carbon nanotubes. *Small* 2005;1(2):180–92.
- [34] Jeon KJ, Moon HR, Ruminski AM, Jiang B, Kisielowski C, Bardhan R, Urban JJ. Air-stable magnesium nanocomposites provide rapid and high-capacity hydrogen storage without using heavy-metal catalysts. *Nat Mater* 2011;10:286–90.
- [35] Miguel-García I, Berenguer-Murcia Ángel, Cazorla-Amorós D. Preferential oxidation of CO catalyzed by supported polymer-protected palladium-based nanoparticles. *Appl Catal B* 2010;98(3–4):161–70.
- [36] He D, Zeng C, Xu C, Cheng N, Li H, Mu S, Pan M. Polyaniline-functionalized carbon nanotube support platinum catalysts. *Langmuir* 2011;27(9):5582–8.
- [37] Li XL, Jia Y, Cao AY. Tailored single-walled carbon nanotube-CdS, nanoparticle hybrids for tunable optoelectronic devices. *ACS Nano* 2010;4(1):506–12.
- [38] Choi HC, Shim M, Bangsaruntip S, Dai H. Spontaneous reduction of metal ions on the sidewalls of carbon nanotubes. *J Am Chem Soc* 2002;124(31):9058–9.
- [39] Grubbs RB. Roles of polymer ligands in nanoparticle stabilization. *Polym Rev* 2007;47(2):197–215.
- [40] Makridis SS, Gkanas EI, Panagakos G, Kikkinides ES, Stubos AK, Wagener P, Barcikowski S. Polymer-stable magnesium nanocomposites prepared by laser ablation for efficient hydrogen storage. *Int J Hydrogen Energy* 2013;38(26):11530–5.
- [41] Benny TH, Pigza JA, Budhoo S, Condon L, Depner SW, Dennis RV, Banerjee S. Synthesis of novel single-walled carbon nanotube-magnesium nanoparticle composites by a solution reduction method. *Mater Lett* 2014;117:305–8.
- [42] Sun YH, Shen CQ, Lai QW, Liu W, Wang DW, Francois K, Zinsoua A. Tailoring magnesium based materials for hydrogen storage through synthesis: current state of the art. *Energy Storage Mater* 2018;10:168–98.
- [43] Paskevicius M, Sheppard DA, Buckley CE. Thermodynamic changes in mechanochemically synthesized magnesium hydride nanoparticles. *J Am Chem Soc* 2010;132(14):5077–83.
- [44] Titus E, Ali N, Cabral G, Gracio, Ramesh JPB, Jackson MJ. Chemically functionalized carbon nanotubes and their characterization using thermogravimetric analysis, fourier transform infrared, and Raman spectroscopy. *J Mater Eng Perform* 2006;15(2):182–6.
- [45] Singh V, Srivastava P, Singh A, Singh D, Malviya T. Polysaccharide-silica hybrids: design and applications. *Polym Rev* 2016;56(1):113–36.
- [46] Zhang J, Zou H, Qing Q, Yang Y, Li Q, Liu Z. Effect of chemical oxidation on the structure of single-walled carbon nanotubes. *J Phys Chem B* 2003;107(16):3712–8.
- [47] Floriano R, Deledda S, Hauback BC, Leiva DR, Botta WJ. Iron and niobium based additives in magnesium hydride: microstructure and hydrogen storage properties. *Int J Hydrogen Energy* 2017;42:6810–9.
- [48] Yuan JG, Zhu YF, Li Y, Li LQ. Effect of multi-wall carbon nanotubes supported palladium addition on hydrogen storage properties of magnesium hydride. *Int J Hydrogen Energy* 2014;39:10184–94.
- [49] Alsabawi K, Webb TA, Mac E, Gray A, Webb CJ. The effect of C60 additive on magnesium hydride for hydrogen storage. *Int J Hydrogen Energy* 2015;40:10508–15.
- [50] Erunal E, Ulusal F, Aslan MY, Guzel B, Uner D. Enhancement of hydrogen storage capacity of multi-walled carbon nanotubes with palladium doping prepared through supercritical CO₂ deposition method. *Int J Hydrogen Energy* 2018;43:10755–64.